Kim, K.-C., Shprits, Y., Blake, J. B. (2016): Fast Injection of the Relativistic Electrons into the Inner Zone and the Formation of the Split-Zone Structure during the Bastille Day Storm in July 2000. - *Journal of Geophysical Research*,*121*, 9, pp. 8329—8342.

DOI: http://doi.org/10.1002/2015JA022072

AGU PUBLICATIONS

JGR

Journal of Geophysical Research: Space Physics

RESEARCH ARTICLE
10.1002/2015JA022072

Key Points:
- SAMPEX observes unusual dynamics of 1 MeV electrons during Bastille Day storm
- HEO-3 and NOAA-15 validates that SAMPEX observations are not contaminated by protons
- Scattering by plasmaspheric hiss produces the observed two-zone split structure

Supporting Information:
- Supporting Information S1

Correspondence to:
K.-C. Kim,
kckim@daegu.ac.kr

Citation:
Kim, K.-C., Y. Y. Shprits, and J. B. Blake (2016), Fast injection of the relativistic electrons into the inner zone and the formation of the split-zone structure during the Bastille Day storm in July 2000, *J. Geophys. Res. Space Physics*, *121*, 8329–8342, doi:10.1002/2015JA022072.

Received 23 OCT 2015
Accepted 12 AUG 2016
Accepted article online 15 AUG 2016
Published online 5 SEP 2016

Fast injection of the relativistic electrons into the inner zone and the formation of the split-zone structure during the Bastille Day storm in July 2000

Kyung-Chan Kim[1], Yuri Y. Shprits[2,3], and J. Bernard Blake[4]

[1]Division of Science Education, College of Education, Daegu University, Gyeongsan, Gyeongbuk, South Korea, [2]Helmholtz Center Potsdam, GFZ, German Research Center For Geosciences, Potsdam, Germany and University of Potsdam, Potsdam, Germany, [3]Department of Earth, Planetary, and Space Sciences, University of California, Los Angeles, California, USA, [4]The Aerospace Corporation, El Segundo, California, USA

Abstract During the July 2000 geomagnetic storm, known as the Bastille Day storm, Solar, Anomalous, and Magnetospheric Particle Explorer (SAMPEX)/Heavy Ion Large Telescope (HILT) observed a strong injection of ~1 MeV electrons into the slot region ($L \sim 2.5$) during the storm main phase. Then, during the following month, electrons were clearly seen diffusing inward down to $L = 2$ and forming a pronounced split structure encompassing a narrow, newly formed slot region around $L = 3$. SAMPEX observations are first compared with electron and proton observations on HEO-3 and NOAA-15 to validate that the observed unusual dynamics was not caused by proton contamination of the SAMPEX instrument. The time-dependent 3-D Versatile Electron Radiation Belt (VERB) simulation of 1 MeV electron flux evolution is compared with the SAMPEX/HILT observations. The results show that the VERB code predicts overall time evolution of the observed split structure. The simulated split structure is produced by pitch angle scattering into the Earth atmosphere of ~1 MeV electrons by plasmaspheric hiss.

1. Introduction

It had been well accepted in the past decades that the Earth's electron radiation belts exhibit a two-zone structure, namely the inner ($L < 2$) and outer zones ($3.5 < L < 8$) with an empty slot region in between. The outer belt is produced by inward radial diffusion [*Kellogg*, 1959] and local acceleration [*Summers et al*., 1998; *Horne and Thorne*, 1998]. *Lyons and Thorne* [1973] modeled the inward radial diffusion in terms of the third invariant in phase space density and loss due to pitch angle scattering by the plasmaspheric hiss. When phase space density was converted into fluxes, the model results appeared to be very similar to that observed by Explorer 45 two-zone structure. The inner electron belt was produced by the balance of very slow radial diffusion and slow loss in the high-density region of the inner zone. Observations by the Van Allen Probes [*Fennell et al*., 2015] showed that in 2012–2015, the fluxes of > 800 keV electron were negligible in the inner belt, indicating that most likely the radial diffusion rates assumed by *Lyons and Thorne* [1973] were unrealistically high. While the quiet structure can be modeled by a simple steady state radial diffusion with loss, during active times outer radiation belt fluxes can vary up to several orders of magnitude on time scales ranging from hours to weeks. The general structure of the ~1 MeV outer electron belt observed in Combined Release and Radiation Effects Satellite (CRRES) has been modeled with the Versatile Electron Radiation Belt (VERB) code [*Shprits et al*., 2008, 2009; *Subbotin and Shprits*, 2009; *Subbotin et al*., 2010]. Comparison of the long-term simulations with CRRES observations [*Subbotin et al*., 2011a; *Kim et al*., 2011a; *Kim and Shprits*, 2013] showed that the code including inward and outward radial diffusion due to ultralow frequency waves, pitch angle, energy, and mixed scattering was capable of reproducing the general dynamics of the outer belt, location of the inner and outer boundary of the radiation belts, and evolution of the peaks in phase space density produced by energy diffusion.

Extreme events and comparison with multienergy observations provide additional challenges for the models and provide a chance to validate the code and may reveal new physical processes. The Solar, Anomalous, and Magnetospheric Particle Explorer (SAMPEX) observed a filling of the initially empty slot region for 2–6 MeV electrons and even into the inner belt ($L < 2.0$) during the "Halloween" storm in 2003 [*Baker et al*., 2004]. The unusual behavior of the outer belt during October–November 2003, when the outer belt was formed inside a slot region, was modeled using 1-D in energy code [*Horne et al*., 2005], 2-D in energy and pitch angle code [*Shprits et al*., 2006a], and 3-D in radial distance pitch angle and energy code

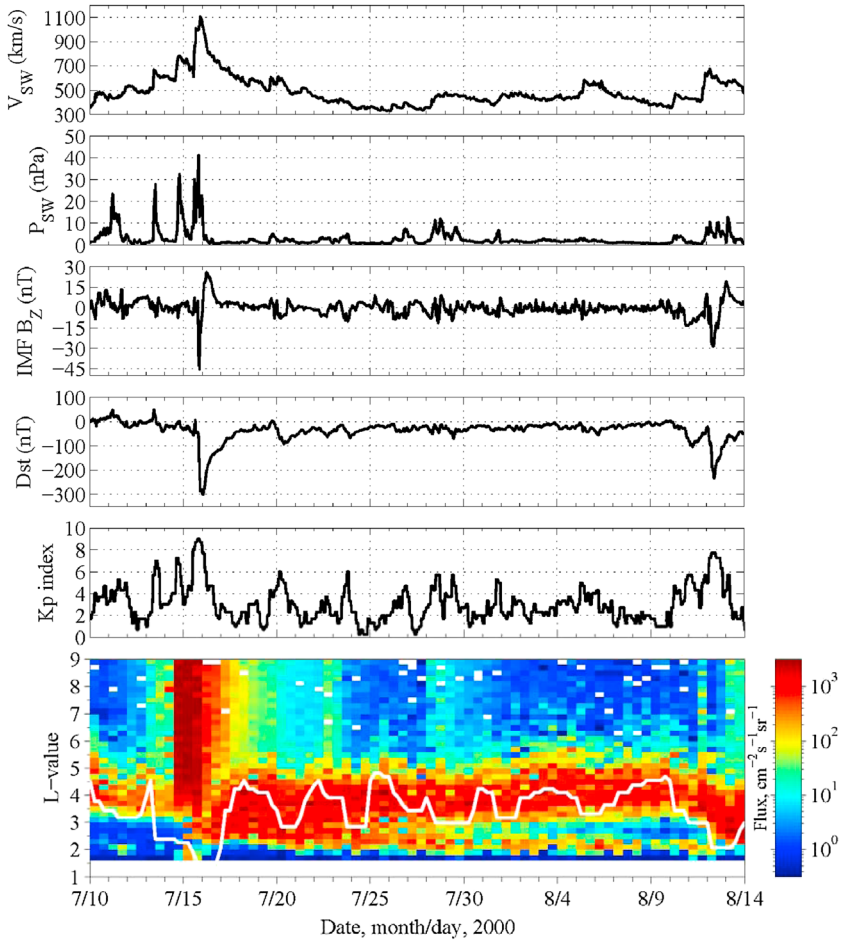

Figure 1. (top to bottom) Evolution of solar wind parameters V_{SW} (km/s), P_{SW} (nPa), IMF B_Z (nT), geomagnetic indices *Dst* (nT), and *Kp* and 12 h average fluxes of the 1 MeV electrons, measured by the SAMPEX/HILT instrument for the time period between 10 July 2000 and 14 August 2000. The location of the plasmapause (white line) is also plotted, calculated following *Carpenter and Anderson* [1992]: $5.6–0.46 \times Kp_{max24}$, where Kp_{max24} is the maximum *Kp* value in the preceding 24 h.

[*Shprits et al.*, 2011]. Simulations showed that local acceleration can play a dominant role for the formation of the outer belt.

Simulations of the dynamics of remnant belts [*Baker et al.*, 2013; *Turner et al.*, 2013] at multi-MeV energies [*Shprits et al.*, 2013] showed that while dynamics of < 2 MeV electrons was well reproduced by the VERB code, electromagnetic ion cyclotron (EMIC) wave scattering was required to reproduce deep dropouts at energies above ~4 MeV. More recently, *Drozdov et al.* [2015], using long-term modeling and comparison with Van Allen Probes observations, showed that EMIC waves provide significant scattering for ultrarelativistic electrons (>4 MeV) even during relatively quiet conditions. Observations of relativistic electrons during March 1991 on CRRES revealed another acceleration mechanism when relativistic electrons were injected into $L = 3$ during the passage of interplanetary shock [*Blake et al.*, 1992; *Li et al.*, 1993]; however, it is inappropriate to conclude that the observations are based only on electrons because of contamination by protons at $L < 2.9$ [*Brautigam*, 2002].

In this study, we report the unusual dynamics of 1 MeV electrons, i.e., a pronounced injection into the slot region ($L < 2$) and following a two-zone split structure, seen by the Heavy Ion Large Telescope (HILT) instrument on board SAMPEX during the July 2000 geomagnetic storms, in particular the so-called Bastille Day Solar Storm.

The paper is organized as follows. In sections 2 and 3, we present the behavior of relativistic electrons and protons measured on the SAMPEX, HEO-3, and NOAA-15 satellites. Then, in section 4, we perform a comparison between model results and SAMPEX observations for 1 MeV electrons. A summary and conclusions are given in section 5.

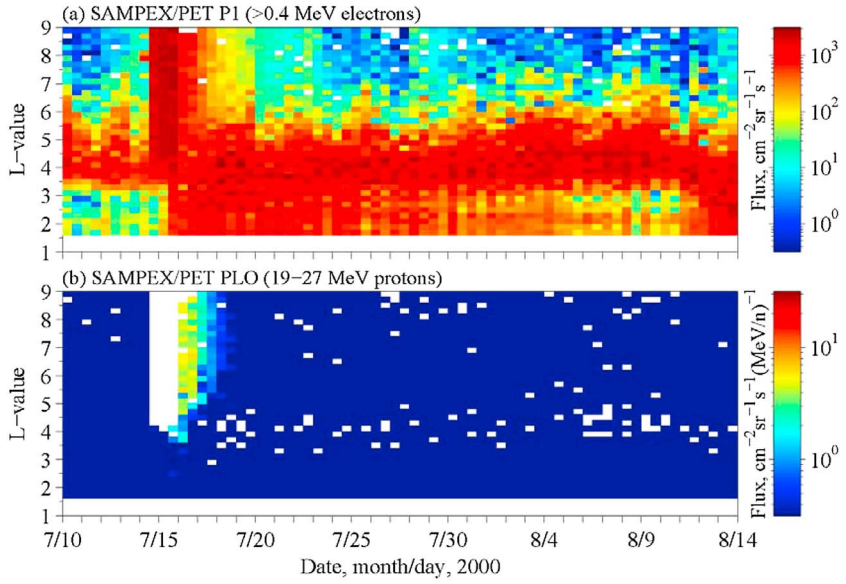

Figure 2. Flux variations measured during the same time interval as in Figure 1 by the SAMPEX/PET P1 channel ((a) >0.4 MeV electrons) and PLO ((b) 19–27 MeV protons). The data are binned in 0.2 *L* values and averaged over 12 h.

2. SAMPEX Observations

Figure 1 (bottom) shows the evolution of 1 MeV electron fluxes observed by the SAMPEX/HILT instrument starting on 10 July 2000, with solar wind and interplanetary magnetic field (IMF) parameters (speed V_{SW}, dynamic pressure P_{SW}, and north-south component of IMF) and geomagnetic indices (*Dst* and *Kp*). During the main phase of the Bastille Day geomagnetic storm (14/15 July 2000), electrons were injected into the slot region ($L \sim 2.5$) and after that were slowly diffusing inward down to $L = 2$. Note that the dynamics of the injected electrons in the center of the inner belt cannot be studied due to severe proton contamination of the HILT instrument. Another interesting fact is that the split structure encompassing a narrow, newly formed slot region around $L = 3$ becomes steadily more pronounced after the storm fully recovered (20 July 2000) and persisted for a month until another strong storm occurred with a *Dst* reaching a value of < -200 nT on 12 August 2000. Losses in the slot region ($2.5 < L < 3.0$) that resides inside the plasmasphere (indicated by a white line) occur on a timescale of several days, which corresponds to that of electron scattering by plasmaspheric hiss [*Abel and Thorne*, 1998a; *Selesnick et al*., 2003; *Meredith et al*., 2007].

Particle measurements by the other SAMPEX sensor, proton/electron telescope (PET) [*Cook et al*., 1993], are also presented in Figure 2 for the same time interval as in Figure 1. Figures 2a and 2b show flux variations, respectively, measured by P1 channel (>400 keV electrons) and PLO (19–27 MeV protons) in the PET. The PET P1 measurements show similar behavior to those seen by the HILT instrument. What is more notable, however, is not only a deeper injection into the region of $L < 2.5$ but also a less pronounced two-zone split structure. By comparing with PET PLO proton data, we can confirm that there is no significant proton contamination in P1 data for the period studied here, except for 16–18 July, possibly suggesting that the flux measured in PET instrument is electrons. The measurements by SAMPEX/HILT will be further validated using electron and proton observations on HEO-3 and NOAA-15 in the next section. In this study, we only focus on the 1 MeV electron dynamics observed by the HILT instrument. Thus, unless otherwise stated herein, SAMPEX observations denote those by the HILT instrument shown in Figure 1.

3. Supporting Observations

3.1. HEO-3 Observations

In this section, we present the evolution of electron and proton fluxes seen by the HEO-3 satellite in order to provide good evidence that solar protons do not contaminate the electron observations made by SAMPEX. Figure 3 shows six energy channels, three for electrons (Ee), > 0.5, > 1.5, and > 3 MeV and three for protons (Ep), > 8, > 16, and > 25 MeV. Note that Ee > 0.5 MeV and Ep > 8 MeV are the same detector with a different

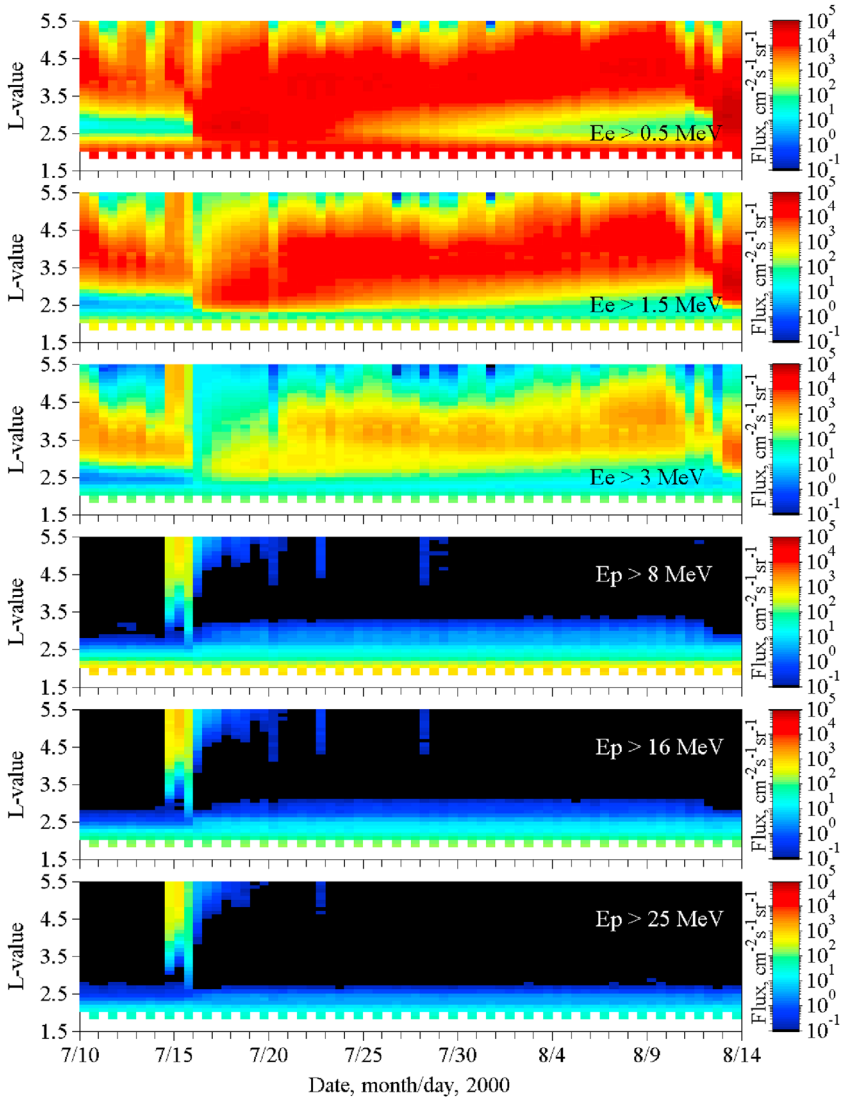

Figure 3. (first to third panels) Electron flux as a function of *L* and time measured on HEO-3 for energies > 0.5, > 1.5, and > 3 MeV and (fourth to sixth panels) proton flux for energies > 8, > 16, and > 25 MeV in the same time interval as Figure 1. Data are averaged over half a day and 0.1 *L* bins.

electronic threshold, likewise for Ee > 1.5 MeV and Ep > 16 MeV, and Ee > 3 MeV and Ep > 25 MeV. This means that when energetic protons are around, they factor in the electron channels, but if the electrons are much more abundant, the proton's influence on count rates is negligible.

Sudden flux enhancements down to $L = 3$ in all energy channels of both electrons and protons are evident during the main phase of the storm, but the electron fluxes are sufficiently higher than those of protons. Except for 14 and 15 July 2000, significant proton fluxes were not seen over all *L* values, especially after the storm fully recovered where the low-orbiting SAMPEX saw the split structure, as described in section 2. It is clear that the dynamics on the electron channel on SAMPEX and HEO are very different from protons on HEO. HEO Ee > 0.5 MeV channel shows a split structure, which is very similar to SAMPEX/HILT observations but is not observed at energies above 1.5 MeV. The observations suggest that there is a threshold energy above which a split structure becomes less pronounced.

For a detailed analysis of the effect of proton contamination, line plots of both electrons and protons around the onset time (14 July 2000) of the storm are presented in Figure 4 (left and right) during the outbound pass and inbound pass of the HEO orbit, respectively. Figure 4 (left) shows that high-energy protons are followed later by lower energy protons. This is the hallmark of an energetic, well-connected event [*Reames*, 1999;

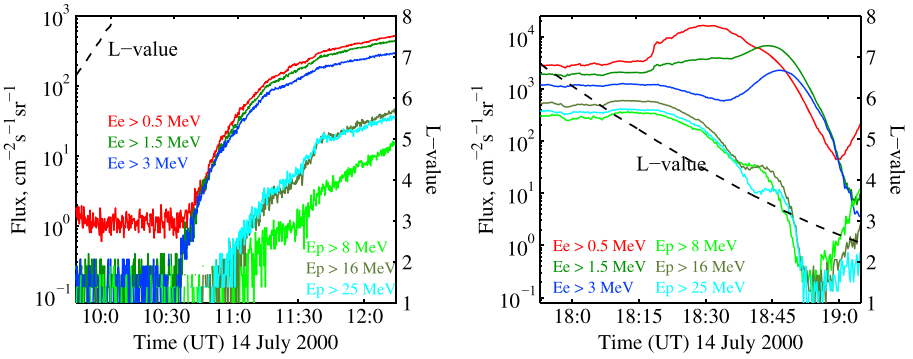

Figure 4. Comparison of electron (>0.5, > 1.5, and > 3 MeV) and proton (>8, > 16, > 25 MeV) channels measured on HEO-3 around the onset time of the Bastille Day event (14 July 2000) during its (left) outbound pass and (right) inbound pass. Note that outbound pass and inbound pass start at UT ~ 8:00 and ~ 14:00, respectively.

Ji et al., 2014]. The high-energy protons arrive first but do not trigger the proton channels because their electronic energy loss (d*E*/d*x*) is too small to trigger. Figure 4 (right) shows that after 18:30 UT, the relativistic electron peaks with higher fluxes than those of protons are nicely seen inside of the proton cutoff around $L \sim 4$, which provides good support for the electron data not being significantly contaminated by protons. These results confirm the conclusion from Figures 3 and 4 that the SAMPEX electron observations are not contaminated by protons.

3.2. NOAA/POES Observations

The NOAA/POES spacecraft orbit the Earth with a Sun-synchronous, near-polar orbit at an altitude of ~ 800–850 km, slightly higher than the SAMPEX's altitude. The SEM (Space Environment Monitor) instrument package on board the NOAA/POES contains solid-state detector telescopes that measure energetic electrons in the energy range 30–2500 keV and protons in the energy range 30–6900 keV [*Evans and Greer*, 2004]. In SEM, the 0° and 90° telescopes are almost orthogonally mounted, with the 0° telescope oriented along the local zenith. Hence, at low latitudes, the 0° telescope measures quasi-trapped particles and the 90° telescope measures precipitating particles, and vice versa at high latitudes. The NOAA-15 P6 proton telescope responds to > 6.9 MeV protons as well as the > 1 MeV electrons it was intended to measure, while its P5 proton telescope exclusively responds to 2.5–6.9 MeV protons [*Miyoshi et al.*, 2008; *Sandanger et al.*, 2009]. Therefore, simultaneous comparisons between the two telescopes make it possible to check whether or not the P6 channel measurements contain high-energy protons. Figures 5a and 5b show measurements from the 0° and 90° telescope, respectively, of the P5 channel. Figures 5c and 5d show measurements from those of the P6 channel. The measurements from the P5 channel show quite different features from those of the P6 channel: (1) no significant count rates in the P5 channel are present for the entire considered time interval, except for the onset time of the storm (14/15 July), in comparison with the P6 channel; and (2) the P6 channel measures many more count rates than those of P5 channel during 14 July. The comparison thus implies that the NOAA-15 P6 proton channel mostly measured >1 MeV electrons for the whole interval. Figure 5b shows a weak flux of 2.5–6.9 MeV protons above approximately $L = 2$. However, a somewhat lower flux exists prior to the injection, and neither SAMPEX nor NOAA-15 P6 sees the prior population, once again indicating that electron measurements on SAMPEX and NOAA-15 are not contaminated by protons.

The electron measurements show similar behavior to those seen by SAMPEX and HEO, although only one of two orthogonal telescopes, the 90° telescope (Figure 5d), detects a faint particle injection into the inner zone at $L < 2$. The NOAA/POES observations serve to validate our argument that the SAMPEX observations are not significantly contaminated by energetic solar protons.

4. Comparison of Simulations With SAMPEX Observations

We have shown above the unusual dynamics of 1 MeV electrons by SAMPEX and validated those by HEO-3 and NOAA-15 during the Bastille Day geomagnetic storm. Now, in order to understand how the split structure around $L \sim 3$, observed on the low-orbiting SAMPEX and shown in the previous section, can be formed, we

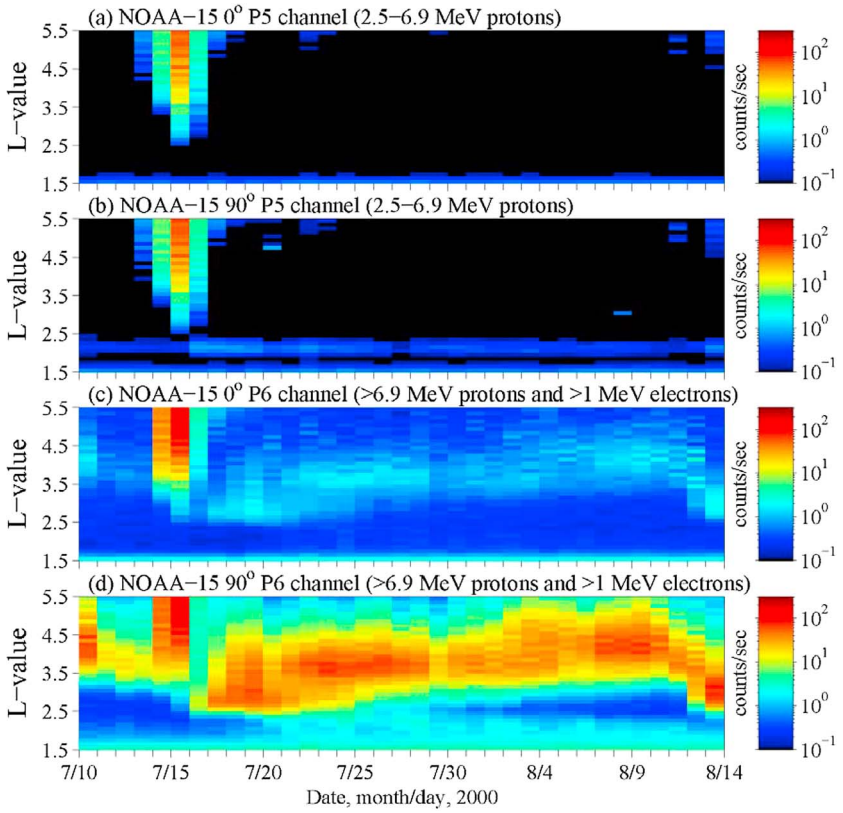

Figure 5. NOAA-15 particle data during the same time interval as in Figure 1, taken from (a and b) the 0° and 90° telescopes of P5 energy channel that measures 2.5–6.9 MeV protons, and from (c and d) the 0° and 90° telescopes of P6 energy channel that measures > 6.9 MeV protons and > 1 MeV electrons. Data are averaged over a day, 0.1 *L* bins, and given in units of counts per seconds.

run the University of California, Los Angeles 3-D VERB code [*Shprits et al.*, 2008; *Subbotin and Shprits*, 2009; *Subbotin et al.*, 2010], which solves the modified Fokker-Planck diffusion equation [*Schulz and Lanzerotti*, 1974; *Shprits et al.*, 2009] as follows:

$$\frac{\partial f}{\partial t} = L^2 \frac{\partial}{\partial L}\Big|_{\mu,J} \left(\frac{1}{L^2} D_{LL} \frac{\partial f}{\partial L}\Big|_{\mu,J} \right) + \frac{1}{T(y)y} \frac{\partial}{\partial y}\Big|_{p,L} T(y) y \left(\langle D_{yy} \rangle \frac{\partial f}{\partial y}\Big|_{p,L} + \langle D_{yp} \rangle \frac{\partial f}{\partial p}\Big|_{y,L} \right) + \frac{1}{p^2} \frac{\partial}{\partial p}\Big|_{y,L} p^2 \left(\langle D_{pp} \rangle \frac{\partial f}{\partial p}\Big|_{y,L} + \langle D_{py} \rangle \frac{\partial f}{\partial y}\Big|_{p,L} \right) - \frac{f}{\tau}, \quad (1)$$

where f is the electron phase space density (PSD); y is the sine of equatorial pitch angle; p is the particle's relativistic momentum; $T(y) = 1.3802 - 0.3198\,(y + y^{1/2})$ [*Lenchek et al.*, 1961]; D_{LL} is the radial diffusion coefficient; $\langle D_{yy} \rangle$, $\langle D_{pp} \rangle$, and $\langle D_{py} \rangle (= \langle D_{yp} \rangle)$ are the bounce- and magnetic local time-averaged pitch angle, momentum, and mixed momentum-pitch angle diffusion coefficients, respectively; τ is a characteristic electron lifetime, equal to a quarter electron bounce period inside the loss cone and assumed to be infinite outside the loss cone. The *Kp*-dependent radial diffusion coefficient produced by electromagnetic field perturbation is adopted from *Brautigam and Albert* [2000]:

$$D_{LL}(Kp, L) = 10^{(0.506Kp - 9.325)} L^{10} \left(\text{day}^{-1} \right). \quad (2)$$

This is valid for $Kp \leq 6$; however, in this study, the parameterization is extrapolated and is used for all *Kp* values. Radial diffusion rates by electrostatic wave fluctuations are not taken into account for our simulation due to their inaccurate dependence of radial diffusion coefficients at lower *L* shell [*Kim et al.*, 2011a; *Ozeke et al.*,

Table 1. Adopted Wave Parameters

Type of Wave	B_w (pT)	λ_{max}	Density Model	MLT Distribution of Wave Power	Wave Spectral Properties	Distribution in Wave Normal
Chorus day	$10^{0.75+0.04\lambda}(2\times10^{0.73+0.91Kp})^{0.5}/57.6$ $Kp\le2+$ $10^{0.75+0.04\lambda}(2\times10^{2.5+0.18Kp})^{0.5}/57.6$ $2+<Kp\le6$	35°	*Sheeley et al.* [2001]	6–12 MLT	$\omega_m/\Omega_e=0.2$ $\delta\omega/\Omega_e=0.1$ $\omega_{uc}/\Omega_e=0.3$ $\omega_{lc}/\Omega_e=0.1$	$\theta_m=0°$ $\delta\theta=30°$ $\theta_{uc}=45°$ $\theta_{lc}=0°$
Chorus night	$50(2\times10^{0.73+0.91Kp})^{0.5}/57.6$ $Kp\le2+$ $50(2\times10^{2.5+0.18Kp})^{0.5}/57.6$ $2+<Kp\le6$	15°	*Sheeley et al.* [2001]	0–6 MLT	$\omega_m/\Omega_e=0.35$ $\delta\omega/\Omega_e=0.15$ $\omega_{uc}/\Omega_e=0.65$ $\omega_{lc}/\Omega_e=0.05$	$\theta_m=0°$ $\delta\theta=30°$ $\theta_{uc}=45°$ $\theta_{lc}=0°$
Plasmaspheric hiss	*Orlova et al.* [2014]	45°	*Denton et al.* [2004, 2006]	6–21 MLT	$f_m=550$ Hz $\delta f=300$ Hz $f_{uc}=2000$ Hz $f_{lc}=100$ Hz	*Thorne et al.* [2013]

2012]. The wave parameters for dayside and nightside chorus and plasmaspheric hiss are presented in Table 1. Based on the parameters in Table 1, the bounce-averaged diffusion coefficients are computed in the centered dipole field model using a quasi-linear approach of *Glauert and Horne* [2005] and *Albert* [2005] for the Landau $n=0$ and $n\le\pm5$ cyclotron resonances for dayside and nightside chorus, and for different resonance numbers depending on energy for plasmaspheric hiss following *Mourenas and Ripoll* [2012]. Our code uses the method of *Orlova and Shprits* [2011] for bounce averaging and integration of uncertainties at mirror points.

The initial conditions are obtained by solving the steady state solution for the radial diffusion equation with a 10 day lifetime and $Kp=2$. The boundary conditions used for this simulation are summarized in Table 2. The numerical grid is $31\times101\times101$, uniform in L and logarithmic in both pitch angle and energy. The PSD variation at the outer boundary ($L=7$) is based on half-day averaged fluxes derived from SAMPEX/HILT 1 MeV at $L=5.5$, which is applied to $L=7$ due to the reason that $L=7$ is likely to be located near the last closed drift path for the simulation interval; thus, boundary fluxes taken at $L=7$ cannot properly account for the source population at the outer L boundary. We use an exponential fit of the energy spectrum of fluxes given by *Shprits et al.* [2006b] as energy-dependent electron distribution at the outer boundary ($L=7$). Following previous studies [e.g., *Subbotin and Shprits*, 2009; *Shprits et al.*, 2009] we scale the energy-dependent PSD by multiplying an energy-independent scaling factor which varies in time. The time-dependent scaling factor is defined as the ratio between the SAMPEX/HILT measurements of 1 MeV electron fluxes over simulation time and the average value of the measurements. We expect that boundary condition derived from the equatorial electron measurements does not make a significant difference in the physical process of producing the split structure in the simulation results below due to the fact that there is the correspondence between the temporal variations of flux in low-altitude orbit and in the equatorial plane [*Baker et al.*, 1994]. We set PSD at the low-energy boundary (10 keV) to be constant, which is obtained by solving the steady state radial diffusion equation used as initial condition. This is based on the fact that the MeV fluxes are relatively insensitive to the fluxes at the low-energy boundary adopted in this study because the first adiabatic invariant corresponding to the energy at the low-energy boundary is too low to provide the seed population for MeV fluxes [*Subbotin et al.*, 2011b]. However, the higher-energy and time-dependent fluxes at the low-energy boundary can lead to significant changes in the MeV fluxes [e.g., *Tu et al.*, 2014], which will be pursued in future. The PSD outside the last closed drift path is set to zero to include the magnetopause shadowing effect

Table 2. Boundary Conditions Used for This Study

Boundary	Conditions	Explanation
$L_{min}=1$	$f=0$	Losses to the atmosphere
$L_{max}=7$	$f=f(t)$	SAMPEX/HILT observations at $L=5.5$
$\alpha_{min}=0.3^o$	$f=0$	Empty loss cone in the weak diffusion regime
$\alpha_{max}=89.7°$	$df/d\alpha=0$	Flat pitch angle distribution at 90°
$E_{min}=10$ keV at L_{max}	$f=$ constant	Balance of convective sources and losses
$E_{max}=10$ MeV at L_{max}	$f=0$	Absence of very high-energy electrons

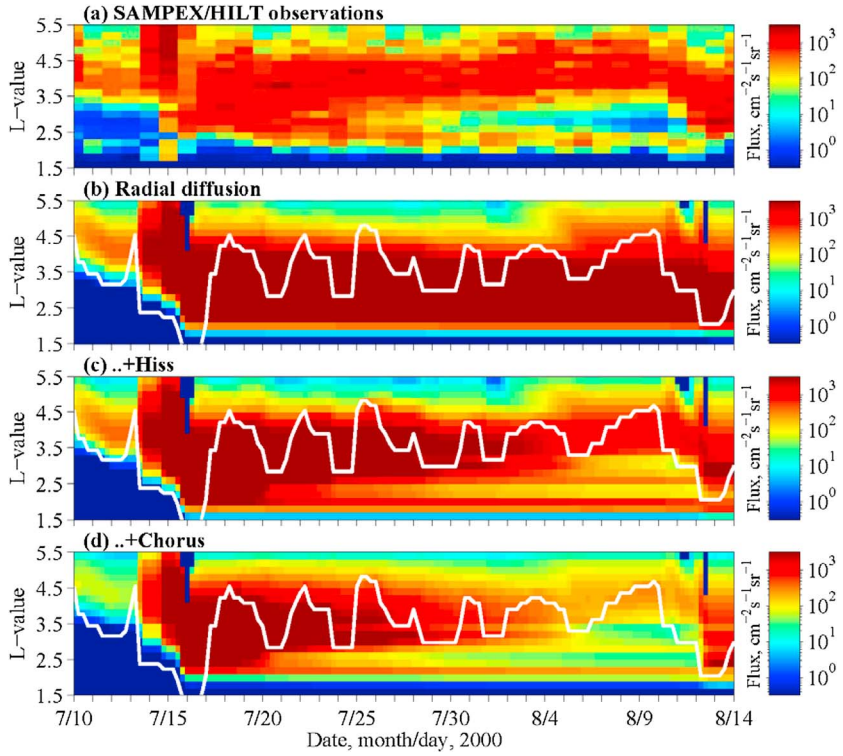

Figure 6. (a) SAMPEX/HILT observations of 1 MeV electron fluxes for the time period between 10 July 2000 and 14 August 2000. (b and d) Time evolution of 1 MeV electron fluxes based on a 3-D VERB diffusion simulation: radial diffusion only (Figure 6b), radial diffusion and pitch angle scattering by plasmaspheric hiss inside the plasmapause (Figure 6c), and pitch angle and energy diffusion including mixed diffusion by chorus waves outside the plasmapause (Figure 6d). The fluxes shown in the simulation are estimated by integrating over the equatorial pitch angles that can reach the SAMPEX altitude.

[*Shprits et al.*, 2006b; *Kim et al.*, 2008, 2010; *Ohtani et al.*, 2009; *Matsumura et al.*, 2011; *Turner et al.*, 2012; *Kim and Lee*, 2014], which will drive subsequent outward radial diffusion by the negative radial PSD gradient [e.g., *Brautigam and Albert*, 2000; *Miyoshi et al.*, 2003; *Shprits et al.*, 2006b; *Kim et al.*, 2011b]. The L value of the last closed path for pitch angle of 90° is estimated from LANL* software [*Yu et al.*, 2012] based on T01s magnetic field model [*Tsyganenko et al.*, 2003]. A more accurate treatment of the magnetopause shadowing effect should be energy dependent and pitch angle dependent, which will be pursued in the future.

Figure 6 shows the results of the sensitivity simulations carried out by adding one-by-one different scattering mechanisms. Note that the maximum value of the y axis (ordinate) in Figure 6 is $L = 5.5$ to focus on the electron dynamics near the split structure, although the outer boundary of the simulation is located at $L = 7$. The SAMPEX/HILT 1 MeV electron observations are shown in Figure 6a for comparison (same as Figure 1, bottom but with a different scale on y axis and daily average fluxes), and the simulated fluxes (J_λ) are estimated by integrating over the equatorial pitch angles (α_0) that can reach the SAMPEX altitude following *Hess* [1968] and are given by

$$J_\lambda = 4\pi \frac{B_\lambda}{B_0} \int_0^{\sin^{-1}\left(\sqrt{B_0/B_\lambda}\right)} j_0(\alpha_0) \frac{\sqrt{\left(1-\sin^2\alpha_0\right)}}{\sqrt{1-(B_\lambda/B_0)\sin^2\alpha_0}} \sin\alpha_0 \mathrm{d}\alpha_0, \tag{3}$$

where B_0 and B_λ are the field intensities at equator and SAMPEX's location in a centered dipole field, respectively.

If only the radial diffusion is included (Figure 6b), then strong injections down to $L < 2$ during the main phase of the Bastille Day geomagnetic storm (14 and 15 July 2000) and the model predict continuously high fluxes in the slot region during the entire simulated time period. Inclusion of pitch angle scattering by plasmaspheric hiss to the radial diffusion model (Figure 6c) gradually reduces the fluxes in the region $2 < L < 3$ inside the plasmapause and reveals the split structure shown in the observations. However, the flux levels outside

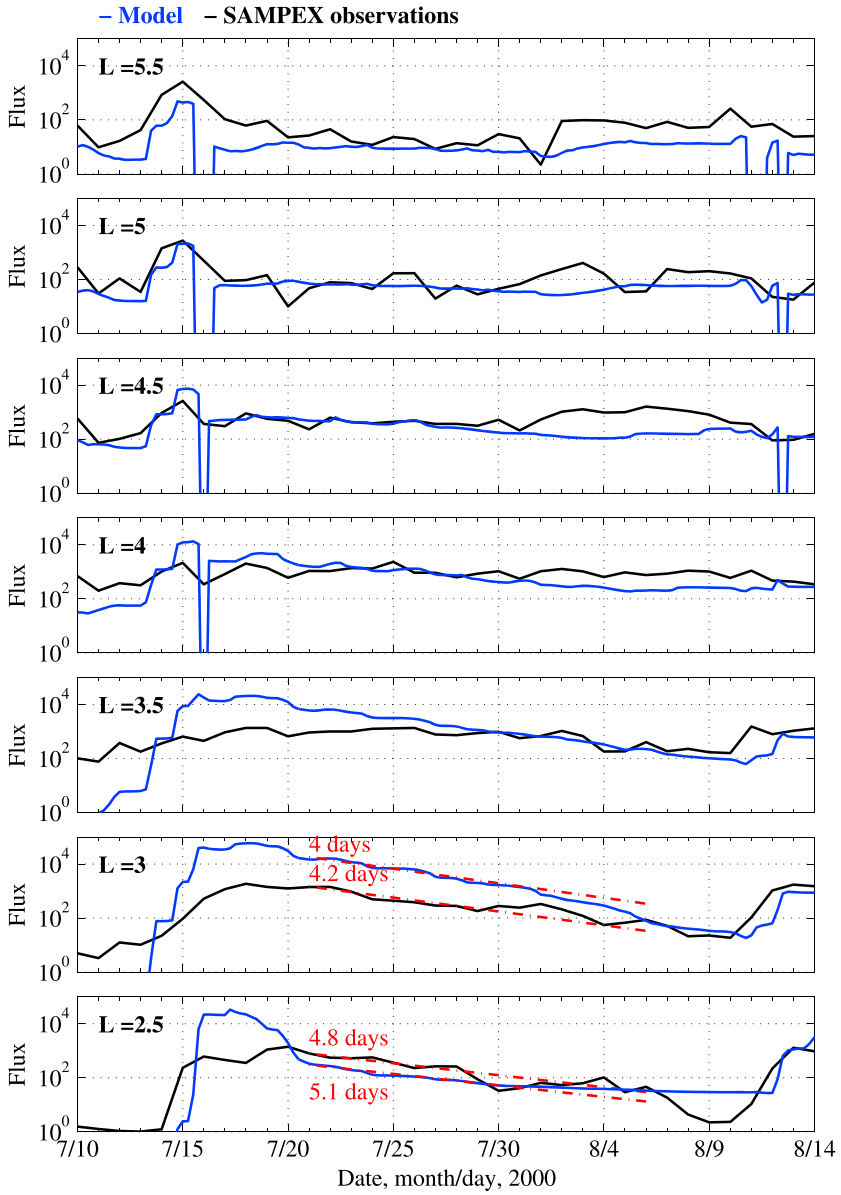

Figure 7. Comparison of electron fluxes modeled by the VERB code simulations with fluxes of 1 MeV electrons observed by SAMPEX/HILT at selected values of *L*. Fluxes are given in units of $cm^{-2}\,s^{-1}\,sr^{-1}$.

the plasmasphere are significantly higher than that of the observation. Introducing chorus waves including pitch angle, momentum, and mixed diffusion outside the plasmasphere lowers the high fluxes, and the flux level becomes more comparable to that in the observations. The flux decrease is due to the substantial loss of fluxes by chorus waves than by hiss waves. In other words, during the storm time (14–17 July 2000), the estimated plasmapause is located deep in the inner region so that pitch angle scattering by chorus waves can be a dominant loss process in the outer radiation belts.

To facilitate a quantitative comparison between the model and data, line plots of the evolution of both the observation and the simulation results at selected *L* values are presented in Figure 7. The simulated results qualitatively agree with the observations in reproducing the split structure, but the quantitative disagreement exists for days around 15–20 July 2000, mostly inside of $L < 4$. More specifically, (1) in the inner region, $L < 4$, the fluxes are roughly 2 orders of magnitude higher than observations, (2) enhancements at low *L* lag observations by more than a day, (3) the low-*L* enhancement penetrates much deeper in the simulation than in the observations, (4) at $L = 2.5$ there is a short-lived (~4 days) peak that is not present in the observations,

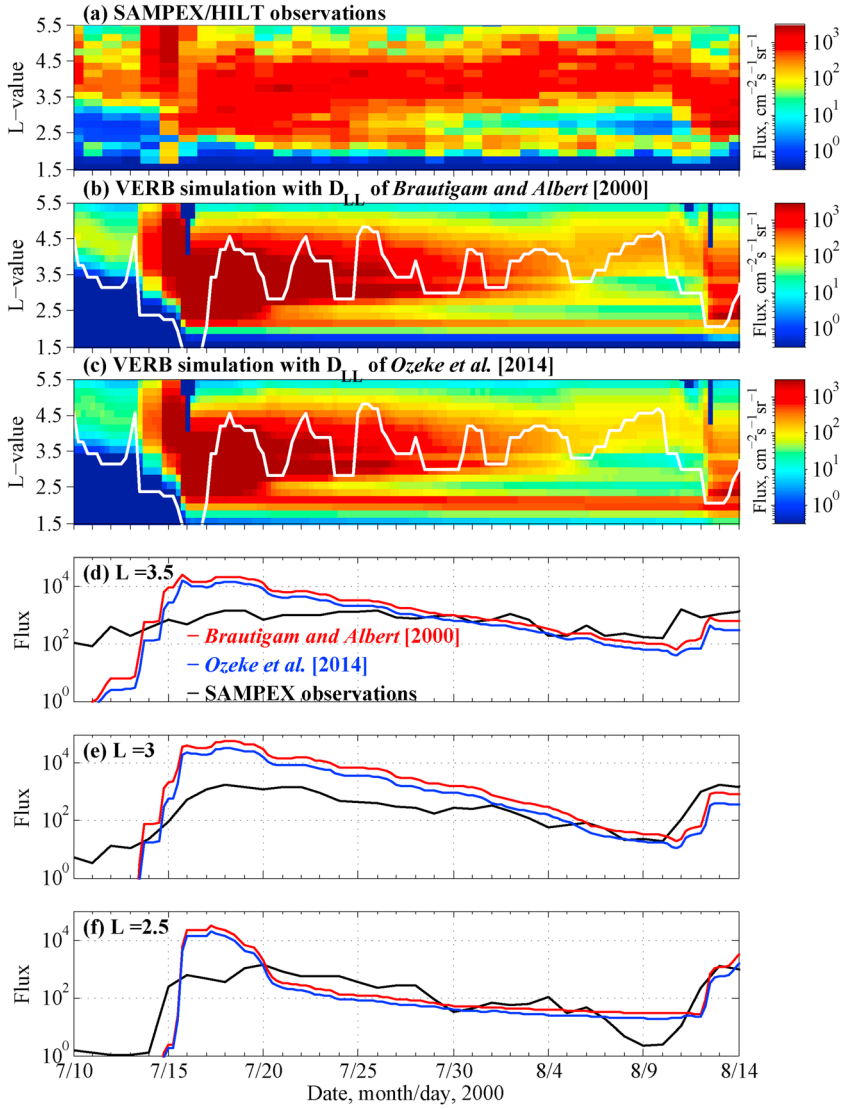

Figure 8. Comparison between simulation results with electromagnetic diffusion coefficient of *Brautigam and Albert* [2000] and with electric and magnetic field diffusion coefficients derived in *Ozeke et al.* [2014]. For more details, see text.

and (5) split structure appears many days earlier in the simulations and the lower *L* enhancement does not appear to propagate inward.

We estimated decay rates of 1 MeV electrons at $L = 2.5$ and 3 where the slot region is pronounced for the period from 21 July to 6 August, which are denoted by the red dotted line in the bottom two panels of Figure 7. The observed decay rates are 4.8 and 4.2 days, respectively, at $L = 2.5$ and 3, which are comparable to 5.1 and 4 days of modeled decay rates. Although VERB code simulation overestimates electron fluxes in the regions for 15–20 July 2000, the comparison of the model with observations, it clearly suggests that the new belt at 1 MeV electrons results from scattering by plasmaspheric hiss.

In *Ozeke et al.* [2014], a new radial diffusion coefficient is determined and compared with that of *Brautigam and Albert* [2000] adopted for this study. They presented that flux enhancements by inward radial diffusion clearly depend to some degree on the choice of diffusion coefficient used, but their diffusion coefficient may not be valid for $Kp > 6$. To investigate how sensitive the model is to the radial diffusion coefficient and the discrepancy between the observed and simulated results in a region of inward of $L < 4$, we perform a simulation with the coefficient of *Ozeke et al.* [2014], including electric and magnetic field perturbations, while our simulation only includes the electromagnetic field perturbation but without electrostatic

perturbation. The simulation result is presented in Figure 8c with observations (Figure 8a) and the result with coefficient of *Brautigam and Albert* [2000] (Figure 8b). A line plot indicating comparison of models and observations at selected values of L is also presented in Figures 8d–8f. We can see from Figure 8 that the replacement of the radial diffusion coefficient does not significantly reduce the fluxes in the regions of $L < 4$, compared to the flux enhancements in the simulation result including that of *Brautigam and Albert* [2000]. However, introduction of the *Ozeke et al*. [2014], diffusion coefficients result in a better agreement in the inner part of the split structure ($L < 2.5$).

Our code generally reproduces the dynamics of the relativistic electrons in the inner belt and the slot region by taking into account only processes that have been considered to be the dominant physical mechanism responsible for the electron radiation belts. It should be noted that there are uncertainties in the amplitudes and spectral characteristics of plasma waves adopted in this study since they are taken from the statistical studies based on the CRRES observations and used electric field measurements. The used parameters may be inaccurate at high levels of geomagnetic activity due to poor data sampling. A more accurate parameterization of the waves should be pursued in the future based on the Van Allen Probes observations with an emphasis on accurate modeling of disturbed geomagnetic conditions. New observations of waves showing different spectral properties of waves [e.g., *Li et al*., 2013, 2015a, 2015b; *Summers et al*., 2014] will be incorporated in future studies. In this study we have not taken into account for pitch angle scattering of electrons by EMIC waves. These waves provide effective pitch angle scattering for multi-MeV electrons, while such scattering may not be effective for the relativistic electrons [*Shprits et al*., 2013; *Sakaguchi et al*., 2013; *Kersten et al*., 2014; *Usanova et al*., 2014; *Drozdov et al*., 2015]. In addition, EMIC waves are excited by the anisotropic ion injections. Since ring current is rarely present below $L = 3$, it is likely that EMIC waves are also not present as such low L shells. For interested readers, the simulation results for different pitch angles and energies in the equatorial region and different boundary condition are included in the supporting information Figures S1–S2.

5. Summary and Conclusions

In this study we have discussed the unusual behavior of 1 MeV electrons seen by SAMPEX/HILT on the Bastille Day geomagnetic storm in 2000 (14/15 July) and during the following month. First, the observations showed a sudden injection of electrons into the slot region ($L < 2.5$), providing a source of the inner belt electrons, followed by a slow inward radial diffusion for approximately a month. The injection occurs well inside the sharp inner boundary for the > 2 MeV belt observed on Van Allen Probes [*Baker et al*., 2014] and well inside the slot region. SAMPEX also shows brief enhancements in electron channel just above $L = 2$. Pitch angle scattering rates at these radial distances are extremely long [*Shprits*, 2009], and the disappearance of these electrons may indicate that these are drift loss cone electrons that were lost during the main phase of the storm. Second, a split in the outer radiation belt was found around $L \sim 3$ inside the plasmasphere after the storm recovery and became more pronounced as time went by. The two-zone split structure is different from that for electron remnant belts [*Baker et al*., 2013; *Turner et al*., 2013; *Shprits et al*., 2013]. For the unusual structure shown in this study, a deep injection is split into two zones, while *Baker et al*. [2013] and *Turner et al*. [2013] showed that a remnant of the preexisting belt and the formation of a new belt result in an apparent two-zone structure in the outer radiation belt. Simultaneous observations by both HEO-3 and NOAA-15 strongly supported our claim that the SAMPEX observations are not significantly contaminated by protons.

We also have compared the features of SAMPEX observations with the 3-D VERB diffusion simulation that includes radial diffusion and pitch angle, energy, and mixed diffusion by chorus waves outside the plasmasphere and pitch angle scattering by plasmaspheric hiss inside the plasmasphere. Our model results generally reproduced the split structure of the 1 MeV electrons in the slot region, implying that plasmaspheric hiss can predominantly remove the electrons injected inside the plasmasphere. However, the model cannot reproduce some of the observed features in the region of $L < 4$, suggesting that a more accurate parameterization using Van Allen Probes observations may improve the results of the simulations due to uncertainty in the wave parameterization adopted in this study. In addition, in this study we have not included another loss from wave-induced scattering inside the plasmasphere due to hiss in plume, lightning-generated whistlers, magnetosonic equatorial noise, and anthropogenic VLF transmitters [e.g., *Abel and Thorne*, 1998a, 1998b; *Summers et al*., 2008; *Meredith et al*., 2009; *Kim et al*., 2011a; *Mourenas et al*., 2013; *Ripoll et al*., 2015]. All these should be incorporated in a future work.

Acknowledgments
We thank the GSFC/SPDF OMNIWeb for provision of the solar wind parameters and geomagnetic activity indices used in this report. We thank Josef Koller for the provision of the LANL* code. HEO-3 particle data were provided to the Virtual Radiation Belt Observatory (ViRBO) by the Aerospace Corporation. SAMPEX particle data were provided from the SAMPEX Data Center at Caltech. We would like to thank Juan Rodriguez for making NOAA-15 particle data available at ftp://satdat.ngdc.noaa.gov/sem/poes/data/. All diffusion coefficients used in this study are available at http://rbm.epss.ucla.edu/.

References

Abel, B., and R. M. Thorne (1998a), Electron scattering loss in Earth's inner magnetosphere: 1. Dominant physical processes, *J. Geophys. Res.*, *103*, 2385–2396, doi:10.1029/97JA02919.

Abel, B., and R. M. Thorne (1998b), Electron scattering loss in Earth's inner magnetosphere: 2. Sensitivity to model parameters, *J. Geophys. Res.*, *103*, 2397–2408, doi:10.1029/97JA02920.

Albert, J. M. (2005), Evaluation of quasi-linear diffusion coefficients for whistler mode waves in a plasma with arbitrary density ratio, *J. Geophys. Res.*, *110*, A03218, doi:10.1029/2004JA010844.

Baker, D. N., J. B. Blake, L. B. Callis, J. R. Cummings, D. Hovestadt, S. Kanekal, B. Klecker, R. A. Mewaldt, and R. D. Zwickl (1994), Relativistic electron acceleration and decay time scales in the inner and outer radiation belts: SAMPEX, *Geophys. Res. Lett.*, *21*(6), 409–412, doi:10.1029/93GL03532.

Baker, D. N., S. G. Kanekal, X. Li, S. P. Monk, J. Goldstein, and J. L. Burch (2004), An extreme distortion of the Van Allen belt arising from the 'Halloween' solar storm in 2003, *Nature*, *432*, 878–881, doi:10.1038/nature03116.

Baker, D. N., et al. (2013), A long-lived relativistic electron storage ring embedded in Earth's outer Van Allen belt, *Science*, *340*, 186–190, doi:10.1126/science.1233518.

Baker, D. N., et al. (2014), An impenetrable barrier to ultra-relativistic electrons in the Van Allen radiation belt, *Nature*, *515*, 531–534, doi:10.1038/nature13956.

Blake, J. B., W. A. Kolasinski, R. W. Fillius, and E. G. Mullen (1992), Injection of electrons and protons with energies of tens of MeV into $L < 3$ on 24 March 1991, *Geophys. Res. Lett.*, *19*(8), 821–824, doi:10.1029/92GL00624.

Brautigam, D. H. (2002), CRRES in review: Space weather and its effects on technology, *J. Atmos. Sol. Terr. Phys.*, *64*, 1709–1721, doi:10.1016/S1364-6826(02)00121-9.

Brautigam, D. H., and J. M. Albert (2000), Radial diffusion analysis of outer radiation belt electrons during the October 9, 1990, magnetic storm, *J. Geophys. Res.*, *105*, 291–310, doi:10.1029/1999JA900344.

Carpenter, D. L., and R. R. Anderson (1992), An ISEE/whistler model of equatorial electron density in the magnetosphere, *J. Geophys. Res.*, *97*, 1097–1108, doi:10.1029/91JA01548.

Cook, W. R., et al. (1993), PET: A proton/electron telescope for studies of magnetospheric, solar, and galactic particles, *IEEE Trans. Geosci. Remote Sens.*, *31*, 565–571.

Denton, R. E., J. D. Menietti, J. Goldstein, S. L. Young, and R. R. Anderson (2004), Electron density in the magnetosphere, *J. Geophys. Res.*, *109*, A09215, doi:10.1029/2003JA010245.

Denton, R. E., K. Takahashi, I. A. Galkin, P. A. Nsumei, X. Huang, B. W. Reinisch, R. R. Anderson, M. K. Sleeper, and W. J. Hughes (2006), Distribution of density along magnetospheric field lines, *J. Geophys. Res.*, *111*, A04213, doi:10.1029/2005JA011414.

Drozdov, A. Y., Y. Y. Shprits, K. G. Orlova, A. C. Kellerman, D. A. Subbotin, D. N. Baker, H. E. Spence, and G. D. Reeves (2015), Energetic, relativistic, and ultrarelativistic electrons: Comparison of long-term VERB code simulations with Van Allen Probes measurements, *J. Geophys. Res. Space Physics*, *120*, 3574–3587, doi:10.1002/2014JA020637.

Evans, D. S., and M. S. Greer (2004), Polar Orbiting Environmental Satellite Space Environment Monitor-2: Instrument descriptions and archive data documentation, *NOAA Tech. Mem. 93*, version 1.4, Space Weather Predict. Cent., Boulder, Colo.

Fennell, J. F., S. G. Claudepierre, J. B. Blake, T. P. O'Brien, J. H. Clemmons, D. N. Baker, H. E. Spence, and G. D. Reeves (2015), Van Allen Probes show that the inner radiation zone contains no MeV electrons: ECT/MagEIS data, *Geophys. Res. Lett.*, *42*, 1283–1289, doi:10.1002/2014GL062874.

Glauert, S. A., and R. B. Horne (2005), Calculation of pitch angle and energy diffusion coefficients with the PADIE code, *J. Geophys. Res.*, *110*, A04206, doi:10.1029/2004JA010851.

Hess, W. N. (1968), *The Radiation Belt and Magnetosphere*, Blaisdell, Waltham, Mass.

Horne, R. B., and R. M. Thorne (1998), Potential waves for relativistic electron scattering and stochastic acceleration during magnetic storms, *J. Geophys. Res.*, *25*(15), 3011–3014, doi:10.1029/98GL01002.

Horne, R. B., et al. (2005), Wave acceleration of electrons in the Van Allen radiation belts, *Nature*, *437*, 227–230, doi:10.1038/nature03939.

Ji, E.-Y., Y.-J. Moon, and J. Park (2014), Forecast of solar proton flux profiles for well-connected events, *J. Geophys. Res. Space Physics*, *119*, 9383–9394, doi:10.1002/2014JA020333.

Kellogg, P. J. (1959), Possible explanation of the radiation observed by Van Allen at high altitudes in satellites, *Nuovo Cimento*, *11*, 48–66, doi:10.1007/BF02724906.

Kersten, T., R. B. Horne, S. A. Glauert, N. P. Meredith, B. J. Fraser, and R. S. Grew (2014), Electron losses from the radiation belts caused by EMIC waves, *J. Geophys. Res. Space Physics*, *119*, 8820–8837, doi:10.1002/2014JA020366.

Kim, K. C., D.-Y. Lee, H.-J. Kim, L. R. Lyons, E. S. Lee, M. K. Öztürk, and C. R. Choi (2008), Numerical calculations of relativistic electron drift loss effect, *J. Geophys. Res.*, *113*, A09212, doi:10.1029/2007JA013011.

Kim, K. C., D.-Y. Lee, H.-J. Kim, E. S. Lee, and C. R. Choi (2010), Numerical estimates of drift loss and *Dst* effect for outer radiation belt relativistic electrons with arbitrary pitch angle, *J. Geophys. Res.*, *115*, A03208, doi:10.1029/2009JA014523.

Kim, K.-C., and D.-Y. Lee (2014), Magnetopause structure favorable for radiation belt electron loss, *J. Geophys. Res. Space Physics*, *119*, 5495–5508, doi:10.1002/2014JA019880.

Kim, K.-C., and Y. Shprits (2013), Long-term relativistic radiation belt electron responses to GEM magnetic storms, *J. Atmos. Sol. Terr. Phys.*, *100–101*, 59–67, doi:10.1016/j.jastp.2013.04.007.

Kim, K.-C., Y. Shprits, D. Subbotin, and B. Ni (2011a), Understanding the dynamic evolution of the relativistic electron slot region including radial and pitch angle diffusion, *J. Geophys. Res.*, *116*, A10214, doi:10.1029/2011JA016684.

Kim, K.-C., D.-Y. Lee, Y. Shprits, H.-J. Kim, and E. Lee (2011b), Electron flux changes in the outer radiation belt by radial diffusion during the storm recovery phase in comparison with the fully adiabatic evolution, *J. Geophys. Res.*, *116*, A09229, doi:10.1029/2011JA016642.

Lenchek, A. M., S. F. Singer, and R. C. Wentworth (1961), Geomagnetically trapped electrons from cosmic ray albedo neutrons, *J. Geophys. Res.*, *66*, 4027–4046, doi:10.1029/JZ066i012p04027.

Li, W., et al. (2013), An unusual enhancement of low-frequency plasmaspheric hiss in the outer plasmasphere associated with substorm-injected electrons, *Geophys. Res. Lett.*, *40*, 3798–3803, doi:10.1002/grl.50787.

Li, W., Q. Ma, R. M. Thorne, J. Bortnik, C. A. Kletzing, W. S. Kurth, G. B. Hospodarsky, and Y. Nishimura (2015a), Statistical properties of plasmaspheric hiss derived from Van Allen Probes data and their effects on radiation belt electron dynamics, *J. Geophys. Res. Space Physics*, *120*, 3393–3405, doi:10.1002/2015JA021048.

Li, W., L. Chen, J. Bortnik, R. M. Thorne, V. Angelopoulos, C. A. Kletzing, W. S. Kurth, and G. B. Hospodarsky (2015b), First evidence for chorus at a large geocentric distance as a source of plasmaspheric hiss: Coordinated THEMIS and Van Allen Probes observation, *Geophys. Res. Lett.*, *42*, 241–248, doi:10.1002/2014GL062832.

Li, X., I. Roth, M. Temerin, J. R. Wygant, M. K. Hudson, and J. B. Blake (1993), Simulation of the prompt energization and transport of radiation belt particles during the March 24, 1991 SSC, *Geophys. Res. Lett.*, *20*(22), 2423–2426, doi:10.1029/93GL02701.

Lyons, L. R., and R. M. Thorne (1973), Equilibrium structure of radiation belt electrons, *J. Geophys. Res.*, *78*, 2142–2149, doi:10.1029/JA078i013p02142.

Matsumura, C., Y. Miyoshi, K. Seki, S. Saito, V. Angelopoulos, and J. Koller (2011), Outer radiation belt boundary location relative to the magnetopause: Implications for magnetopause shadowing, *J. Geophys. Res.*, *116*, A06212, doi:10.1029/2011JA016575.

Meredith, N. P., R. B. Horne, S. A. Glauert, and R. R. Anderson (2007), Slot region electron loss timescales due to plasmaspheric hiss and lightning-generated whistlers, *J. Geophys. Res.*, *112*, A08214, doi:10.1029/2007JA012413.

Meredith, N. P., R. B. Horne, S. A. Glauert, D. N. Baker, S. G. Kanekal, and J. M. Albert (2009), Relativistic electron loss timescales in the slot region, *J. Geophys. Res.*, *114*, A03222, doi:10.1029/2008JA013889.

Miyoshi, Y., A. Morioka, T. Obara, H. Misawa, T. Nagai, and Y. Kasahara (2003), Rebuilding process of the outer radiation belt during the 3 November 1993 magnetic storm: NOAA and Exos-D observations, *J. Geophys. Res.*, *108*(A1), 1004, doi:10.1029/2001JA007542.

Miyoshi, Y., K. Sakaguchi, K. Shiokawa, D. Evans, J. Albert, M. Connors, and V. Jordanova (2008), Precipitation of radiation belt electrons by EMIC waves, observed from ground and space, *Geophys. Res. Lett.*, *35*, L23101, doi:10.1029/2008GL035727.

Mourenas, D., and J.-F. Ripoll (2012), Analytical estimates of quasi-linear diffusion coefficients and electron lifetimes in the inner radiation belt, *J. Geophys. Res.*, *117*, A01204, doi:10.1029/2011JA016985.

Mourenas, D., A. V. Artemyev, O. V. Agapitov, and V. Krasnoselskikh (2013), Analytical estimates of electron quasi-linear diffusion by fast magnetosonic waves, *J. Geophys. Res. Space Physics*, *118*, 3096–3112, doi:10.1002/jgra.50349.

Ohtani, S., Y. Miyoshi, H. J. Singer, and J. M. Weygand (2009), On the loss of relativistic electrons at geosynchronous altitude: Its dependence on magnetic configurations and external conditions, *J. Geophys. Res.*, *114*, A01202, doi:10.1029/2008JA013391.

Orlova, K. G., and Y. Y. Shprits (2011), On the bounce-averaging of scattering rates and the calculation of bounce period, *Phys. Plasmas*, *18*, 092,904, doi:10.1063/1.363813.

Orlova, K., M. Spasojevic, and Y. Shprits (2014), Activity-dependent global model of electron loss inside the plasmasphere, *Geophys. Res. Lett.*, *41*, 3744–3751, doi:10.1002/2014GL060100.

Ozeke, L. G., I. R. Mann, K. R. Murphy, I. J. Rae, and A. A. Chan (2012), ULF wave-driven radial diffusion simulation of the outer radiation belt, in *Dynamics of the Earth's Radiation Belts and Inner Magnetosphere*, *Geophys. Monogr. Ser.*, vol. 199, edited by D. Summers et al., pp.139–149, AGU, Washington, D. C., doi:10.1029/2012GM001332.

Ozeke, L. G., I. R. Mann, K. R. Murphy, I. Jonathan Rae, and D. K. Milling (2014), Analytic expressions for ULF wave radiation belt radial diffusion coefficients, *J. Geophys. Res. Space Physics*, *119*, 1587–1605, doi:10.1002/2013JA019204.

Reames, D. V. (1999), Particle acceleration at the Sun and in the heliosphere, *Space Sci. Rev.*, *90*, 413–491.

Ripoll, J.-F., Y. Chen, J. F. Fennell, and R. H. W. Friedel (2015), On long decays of electrons in the vicinity of the slot region observed by HEO3, *J. Geophys. Res. Space Physics*, *120*, 460–478, doi:10.1002/2014JA020449.

Sakaguchi, K., Y. Kasahara, M. Shoji, Y. Omura, Y. Miyoshi, T. Nagatsuma, A. Kumamoto, and A. Matsuoka (2013), Akebono observations of EMIC waves in the slot region of the radiation belts, *Geophys. Res. Lett.*, *40*, 5587–5591, doi:10.1002/2013GL058258.

Sandanger, M. I., F. Soraas, M. Sorbo, K. Aarsnes, K. Oksavik, and D. S. Evans (2009), Relativistic electron losses related to EMIC waves during CIR and CME storms, *J. Atmos. Sol. Terr. Phys.*, *71*, 1126–1144, doi:10.1016/j.jastp.2008.07.006.

Schulz, M., and L. Lanzerotti (1974), *Particle Diffusion in the Radiation Belts*, *Phys. Chem. Space*, vol. 7, Springer, New York.

Selesnick, R. S., J. B. Blake, and R. A. Mewaldt (2003), Atmospheric losses of radiation belt electrons, *J. Geophys. Res.*, *108*(A12), 1468, doi:10.1029/2003JA010160.

Sheeley, B., M. Moldwin, H. Rassoul, and R. Anderson (2001), An empirical plasmasphere and trough density model: CRRES observations, *J. Geophys. Res.*, *106*, 25,631–25,641, doi:10.1029/2000JA000286.

Shprits, Y. Y. (2009), Potential waves for pitch-angle scattering of near-equatorially mirroring energetic electrons due to the violation of the second adiabatic invariant, *Geophys. Res. Lett.*, *36*, L12106, doi:10.1029/2009GL038322.

Shprits, Y. Y., R. M. Thorne, R. B. Horne, S. A. Glauert, M. Cartwright, C. T. Russell, D. N. Baker, and S. G. Kanekal (2006a), Acceleration mechanism responsible for the formation of the new radiation belt during the 2003 Halloween solar storm, *Geophys. Res. Lett.*, *33*, L05104, doi:10.1029/2005GL024256.

Shprits, Y. Y., R. M. Thorne, R. Friedel, G. D. Reeves, J. Fennell, D. N. Baker, and S. G. Kanekal (2006b), Outward radial diffusion driven by losses at magnetopause, *J. Geophys. Res.*, *111*, A11214, doi:10.1029/2006JA011657.

Shprits, Y. Y., D. A. Subbotin, N. P. Meredith, and S. R. Elkington (2008), Review of modeling of losses and sources of relativistic electrons in the outer radiation belts: II. Local acceleration and loss, *J. Atmos. Sol. Terr. Phys.*, *70*(14), 1694–1713, doi:10.1016/j.jastp.2008.06.014.

Shprits, Y. Y., D. Subbotin, and B. Ni (2009), Evolution of electron fluxes in the outer radiation belt computed with the VERB code, *J. Geophys. Res.*, *114*, A11209, doi:10.1029/2008JA013784.

Shprits, Y. Y., D. Subbotin, A. Drozdov, M. E. Usanova, A. Kellerman, K. Orlova, D. N. Baker, D. L. Turner, and K.-C. Kim (2013), Unusual stable trapping of the ultrarelativistic electrons in the Van Allen radiation belts, *Nat. Phys.*, doi:10.1038/nphys2760.

Shprits, Y., D. Subbotin, B. Ni, R. Horne, D. Baker, and P. Cruce (2011), Profound change of the near-Earth radiation environment caused by solar superstorms, *Space Weather*, *9*, S08007, doi:10.1029/2011SW000662.

Subbotin, D. A., and Y. Y. Shprits (2009), Three-dimensional modeling of the radiation belts using the Versatile Electron Radiation Belt (VERB) code, *Space Weather*, *7*, S10001, doi:10.1029/2008SW000452.

Subbotin, D. A., Y. Y. Shprits, and B. Ni (2011a), Long-term radiation belt simulation with the VERB 3-D code: Comparison with CRRES observations, *J. Geophys. Res.*, *116*, A12210, doi:10.1029/2011JA017019.

Subbotin, D. A., Y. Y. Shprits, M. Gkioulidou, L. R. Lyons, B. Ni, V. G. Merkin, F. R. Toffoletto, R. M. Thorne, R. Horne, and M. K. Hudson (2011b), Simulation of the acceleration of relativistic electrons in the inner magnetosphere using RCM-VERB coupled codes, *J. Geophys. Res.*, *116*, A08211, doi:10.1029/2010JA016350.

Subbotin, D., Y. Shprits, and B. Ni (2010), Three-dimensional VERB radiation belt simulations including mixed diffusion, *J. Geophys. Res.*, *115*, A03205, doi:10.1029/2009JA015070.

Summers, D., R. M. Thorne, and F. Xiao (1998), Relativistic theory of wave-particle resonant diffusion with application to electron acceleration in the magnetosphere, *J. Geophys. Res.*, *103*(A9), 20,487–20,500, doi:10.1029/98JA01740.

Summers, D., B. Ni, N. P. Meredith, R. B. Horne, R. M. Thorne, M. B. Moldwin, and R. R. Anderson (2008), Electron scattering by whistler-mode ELF hiss in plasmaspheric plumes, *J. Geophys. Res.*, *113*, A04219, doi:10.1029/2007JA012678.

Summers, D., Y. Omura, S. Nakamura, and C. A. Kletzing (2014), Fine structure of plasmaspheric hiss, *J. Geophys. Res. Space Physics*, *119*, 9134–9149, doi:10.1002/2014JA020437.

Thorne, R. M., et al. (2013), Evolution and slow decay of an unusual narrow ring of relativistic electrons near $L \sim 3.2$ following the September 2012 magnetic storm, *Geophys. Res. Lett.*, *40*, 3507–3511, doi:10.1002/grl.50627.

Tsyganenko, N. A., H. J. Singer, and J. C. Kasper (2003), Storm-time distortion of the inner magnetosphere: How severe can it get?, *J. Geophys. Res.*, *108*(A5), 1209, doi:10.1029/2002JA009808.

Tu, W., G. S. Cunningham, Y. Chen, S. K. Morley, G. D. Reeves, J. B. Blake, D. N. Baker, and H. Spence (2014), Event-specific chorus wave and electron seed population models in DREAM3D using the Van Allen Probes, *Geophys. Res. Lett.*, *41*, 1359–1366, doi:10.1002/2013GL058819.

Turner, D. L., Y. Y. Shprits, M. Hartinger, and V. Angelopoulos (2012), Explaining sudden losses of outer radiation belt electrons during geomagnetic storms, *Nat. Phys.*, *8*, 208–212, doi:10.1038/nphys2185.

Turner, D. L., V. Angelopoulos, W. Li, M. D. Hartinger, M. Usanova, I. R. Mann, J. Bortnik, and Y. Shprits (2013), On the storm-time evolution of relativistic electron phase space density in Earth's outer radiation belt, *J. Geophys. Res. Space Physics*, *118*, 2196–2212, doi:10.1002/jgra.50151.

Usanova, M. E., et al. (2014), Effect of EMIC waves on relativistic and ultrarelativistic electron populations: Ground-based and Van Allen Probes observations, *Geophys. Res. Lett.*, *41*, 1375–1381, doi:10.1002/2013GL059024.

Yu, Y., J. Koller, S. Zaharia, and V. Jordanova (2012), L^* neural networks from different magnetic field models and their applicability, *Space Weather*, *10*, S02014, doi:10.1029/2011SW000743.